LANGMUIR Article
Cite This: Langmuir 2019, 35, 10461−10474
pubs.acs.org/Langmuir

Construction and Evaluation of a Self-Calibrating Multiresponse and Multifunctional Graphene Biosensor

Siamak Beyranvand,[†] Mohammad F. Gholami,[‡] Abbas D. Tehrani,[†] Jürgen P. Rabe,[‡] and Mohsen Adeli*[,†]

[†]Department of Chemistry, Faculty of Science, Lorestan University, Khorramabad, Iran
[‡]Department of Physics and IRIS Adlershof, Humboldt-Universität zu Berlin, Berlin, Germany

Supporting Information

ABSTRACT: Recently, many studies have been focused on the development of graphene-based biosensors. However, they rely on one type of signal and need to be calibrated by other techniques. In this study, a nonenzymatic graphene-based biosensor has been designed and constructed. Its ability to detect glucose and *Escherichia coli* by three different types of signals has been investigated. For its preparation, dopamine-functionalized polyethylene glycol and 2,5-thiophenediylbisboronic acid were conjugated onto the surface of graphene sheets by nitrene [2 + 1] cycloaddition and condensation reactions, respectively. Multivalent interactions between boronic acid segments and biosystems consequently increased the quantifiable fluorescence emission and UV absorption of dopamine segments. Additionally, changing the electrochemical behavior of the functionalized graphene sheets was possible and resulted in a measurable output signal. Conjugation of mannose onto the surface of the biosensor improved its magnitude of signals and specificity for sensing *E. coli* in a complex medium. The efficiency and accuracy of each signal was monitored by others, which resulted in a real-time self-calibrating biosensor. Taking advantage of the versatility of the three different indicators, including florescence, UV, and electrochemistry, the functionalized graphene sheets have been used as self-regulating biosensors to detect a variety of biosystems with a high accuracy and specificity in a short time.

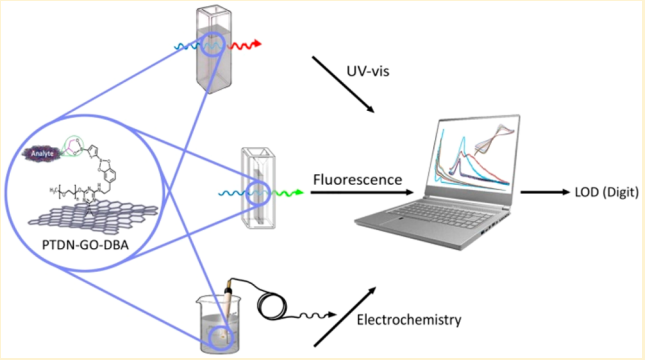

INTRODUCTION

Biosensors are analytical devices with a fast response and ability to directly convert biointeractions to quantifiable and processable physiochemical signals.[1−3] They are used for sensing different analytes ranging from small molecules, e.g., saccharides,[4] to large objects including glycans,[5] nucleic acids,[6] proteins,[7] pathogens,[8] and cancer cells.[9] Usually biosensors consist of interacting functional groups and detectors assembled on a platform.[10] Two-dimensional (2D) nanomaterials are of great interest as sensor platforms because of their unique mechanical and physicochemical properties.[11,12] Graphene derivatives including graphene oxide (GO), reduced graphene oxide (rGO), and graphene quantum dots (GQDs) are the most versatile platforms that have been used to construct biosensors.[13−20] Due to their huge surface area, flexibility, and optoelectronic properties, they are able to improve the sensitivity, response time, and limit of detection of biosensors efficiently.[21−23] In the graphene-based sensors, detectors can be attached to the graphene platform either by covalent or by noncovalent approaches.[24−29] Functionality is one of the key factors that improves the sensibility of graphene-based sensors.[30] A large number of interactive functional groups that are conjugated to the surface of graphene platforms cause strong multivalent interactions with biosystems[31−35] and amplify the intensity of detector signal. (Macro)molecules with a boronic acid functionality have been widely applied for the fabrication of biosensors.[36,37] They are able to bind to *cis*-1,2- and 1,3-diols of different biosystems such as carbohydrates, proteins, and pathogens at alkaline conditions. Lipopolysaccharides, as the basic components of the external cell wall of Gram-negative bacteria,[38] are able to attach to boronic acids through which these microorganisms can be detected.[39] It has been reported that boronic acid segments noncovalently immobilized on graphene sheets were successfully able to sense glucose molecules.[40,41] However, low stability of the boronic acid functional groups that are attached to the surface of graphene noncovalently hamper application of such systems at physiological and complex media. This could be a drawback, particularly when sensing large biosystems such as pathogens that are able to separate boronic acids from the surface of graphene sheets. Therefore, covalent attachment of boronic acid functionalities to the surface of graphene sheets improves the efficiency of such biosensors.

Received: March 28, 2019
Revised: June 5, 2019
Published: July 22, 2019

DOI: 10.1021/acs.langmuir.9b00915
Langmuir 2019, 35, 10461−10474

Scheme 1. (a) Synthesis of Telechelic Polymer by Stepwise Functionalization of Poly(ethylene glycol);[a] (b) Modification of nGO by Telechelic Polymer through Nitrene [2 + 1] Cycloaddition Reaction at 100 °C for 48 h in DMF; (c) Condensation of 2,5-Thiophenediylbis-boronic Acid with the Dopamine Groups of Modified nGO at 50 °C for 24 h in DMF Resulted in Boronic Acid-Functionalized Nanosheets

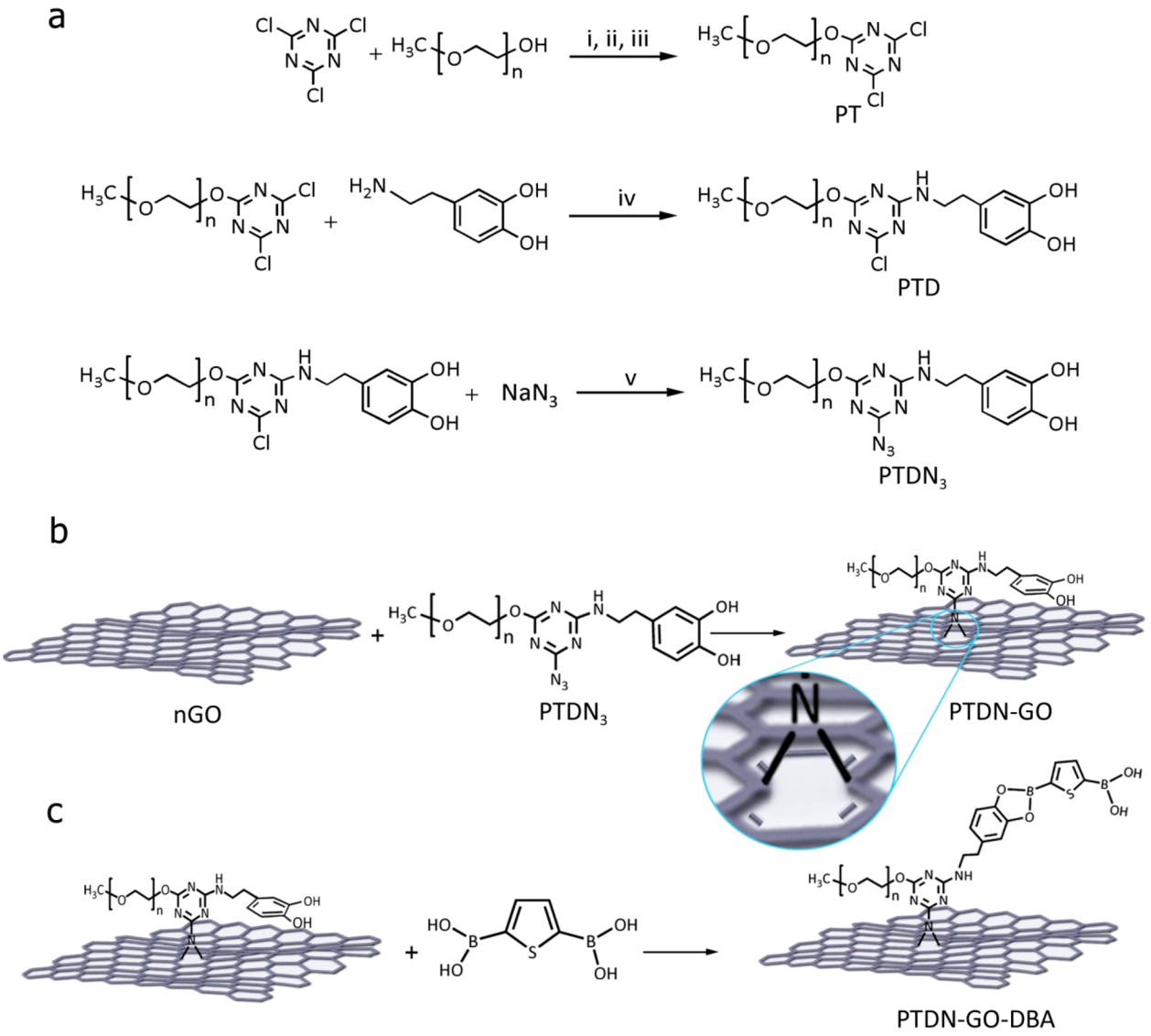

[a]Conditions: (i) 0 °C, 1 h, dichloromethane. (ii) rt, 1 h. (iii) 50 °C, 12 h. (iv) rt, 12 h, H_2O. (v) 80 °C, 48 h, H_2O.

Catechol derivatives such as dopamine are another class of materials that strongly bind to boronic acids.[42] Dopamine is a catecholamine neurotransmitter that plays several important roles in the brain and body.[43,44] In addition, it shows redox property and can be oxidized by different oxidants to dopaquinone.[45] It shows a fluorescence emission at 330 nm when excited at 266 nm.[46,47] Therefore, both the electrochemical properties and the fluorescence signals of dopamine can be also used as indicators to detect different biosystems.[48,49] As a result, controlled and covalent attachment of boronic acid/dopamine combinations onto the surface of graphene sheets leads to new biosensors with the ability of multivalent interactions and detecting biosystems. However, in situ calibration of biosensors still is an unsolved problem, which should be overcome to obtain real-time signals with a high accuracy.[50] In order to quantify and standardize a biosensor signal it should be calibrated by other techniques. In most cases, the calibration technique is not compatible with the interacting interfaces and sensing conditions.

In this work, we solved this problem by constructing a multiresponse graphene-based sensor. A telechelic polymer with dopamine and azide functionalities has been synthesized and attached to the surface of graphene by nitrene [2 + 1] cycloaddition reaction. Then functionalized graphene sheets were modified by 2,5-thiophenediylbisboronic acid, and 2D nanomaterials with boronic acid functionalities were obtained. Interactions between boronic acid groups and *cis*-1,2- or 1,3-diols of biosystems changed the fluorescence emission, UV absorption, and electrochemical behavior of the functionalized graphene sheets. Changes in these optoelectronic properties were then used as signals to detect glucose and *E. coli*. Signal and specificity of this biosensor for detection of *E. coli* in a complex media were efficiently improved by conjugating mannose onto its surface. The accuracy of each signal was tested by other

DOI: 10.1021/acs.langmuir.9b00915
Langmuir 2019, 35, 10461−10474

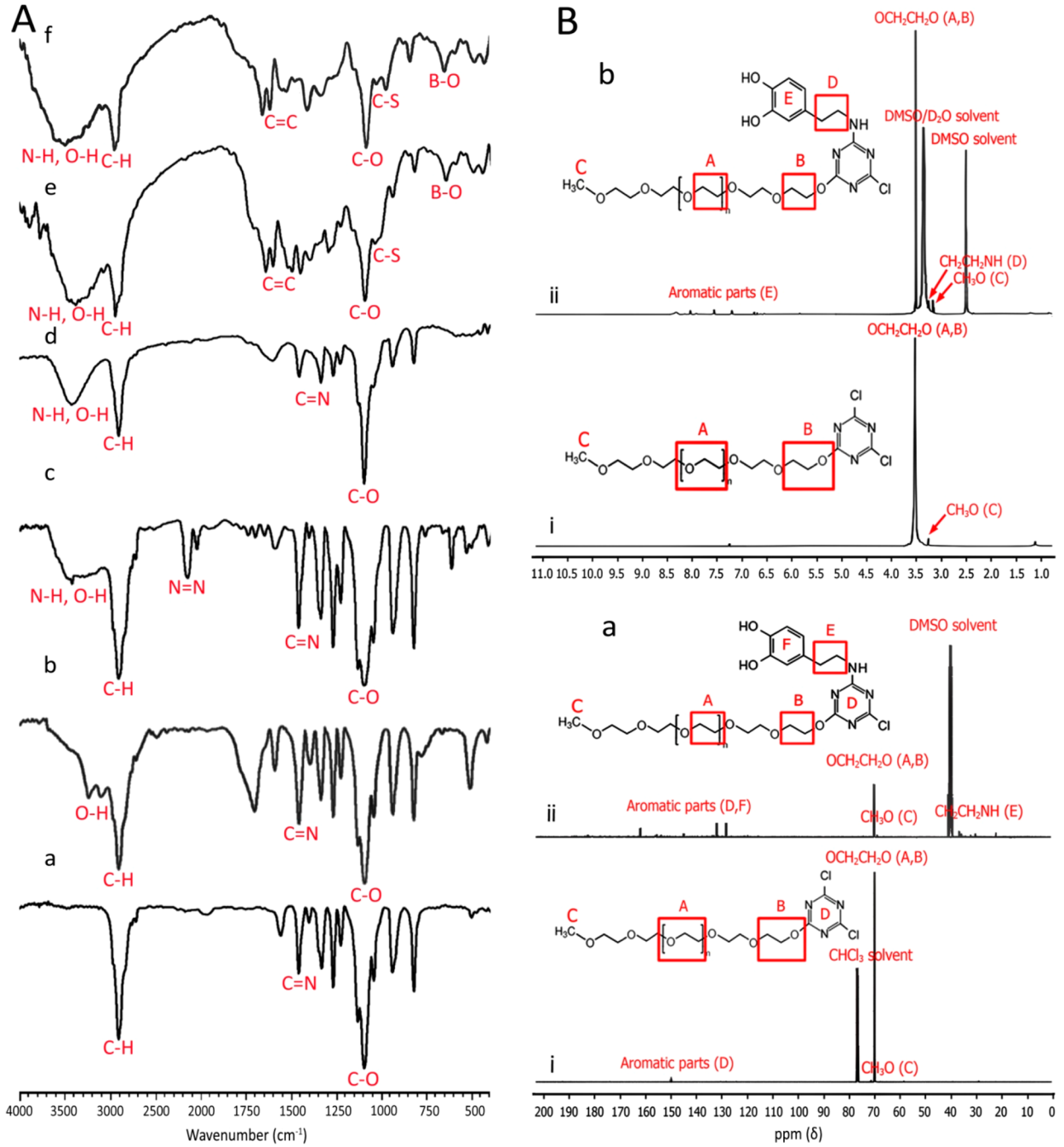

Figure 1. (A) FT-IR spectra of (a) PT, (b) PTD, (c) $PTDN_3$, (d) PTDN-GO, (e) PTDN-GO-DBA, and (f) PTDN-GO-DBA-Mann. (B) (a) ^1H NMR spectra of (i) PT and (ii) PTD in DMSO-d_6. Signals of different segments are shown on spectra. (b) ^{13}C NMR spectra of (i) PT and (ii) PTD in chloroform. Signal of the carbon atoms of the triazine groups did not appear due to the lack of NOE effect. However, the signal of the dopamine segment could be clearly seen.

signals, which led to a self-calibrating biosensor with high versatility to detect different biosystems.

EXPERIMENTAL SECTION

Full information including materials, instruments, and synthetic protocols is available in the experimental section of the Supporting Information.

RESULTS AND DISCUSSION

In this work, a new type of graphene-based biosensor using our recently published procedure for the controlled functionalization of graphene sheets[51−53] has been reported.

Table 1. Element Analysis of the Functionalized nGO Derivatives[a]

compound	C (%)	H (%)	N (%)	S (%)
PTDN3	41.2	6.7	1.9	
nGO	41.4	2.2		
PTDN-GO	43.5	3.2	1.4	
PTDN-GO-DBA	41.2	4.7	1.1	1.1
PTDN-GO-DBA-Mann	43.3	2.7	0.9	1.1

[a]The high hydrogen content for PTDN-GO, PTDN-GO-DBA, and PTDN-GO-DBA-Mann is due to the trapped water.

DOI: 10.1021/acs.langmuir.9b00915
Langmuir 2019, 35, 10461−10474

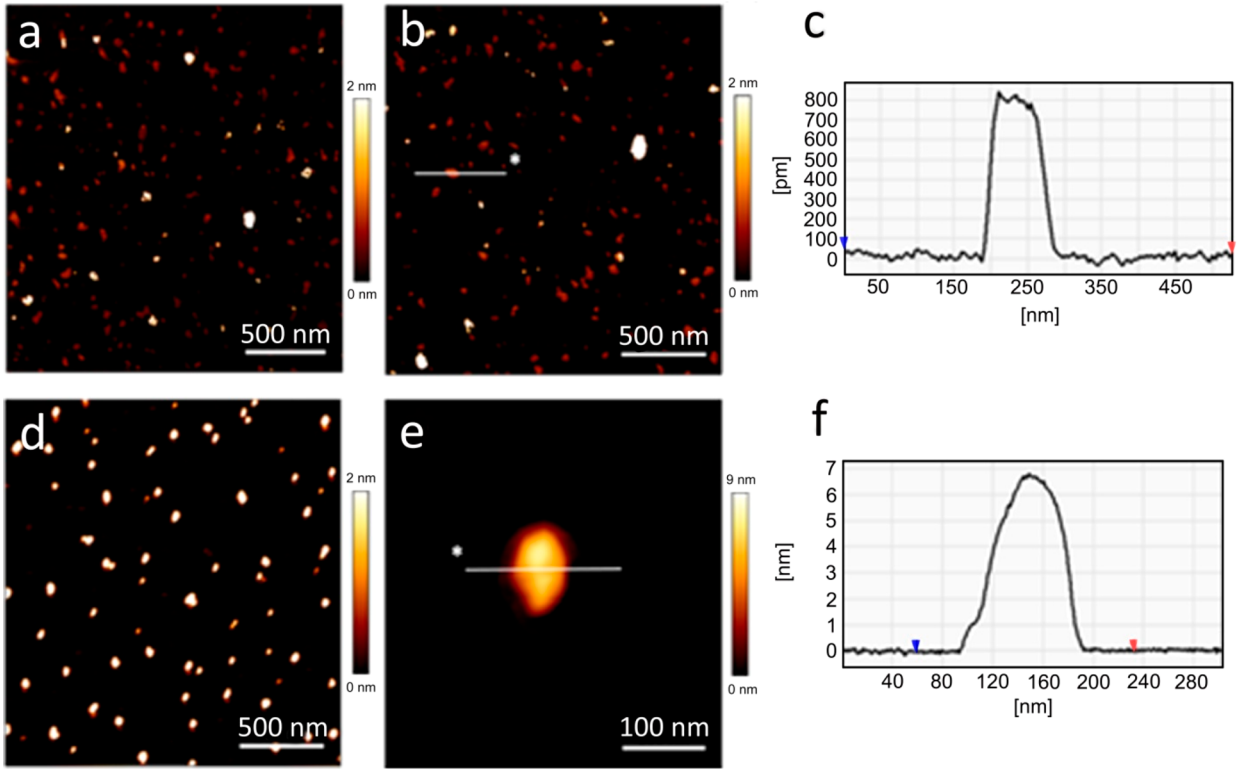

Figure 2. TM-SFM height images of (a and b) nGO sheets deposited from water dispersion onto the freshly cleaved mica surface. (c) Line profile of a typical nGO sheet as deposited onto mica flat surface. (d and e) PTDN-GO-DBA nanostructures deposited from water dispersion onto freshly cleaved mica surface. (e) Higher magnification of PTDN-GO-DBA nanostructure. (f) Height profile of a single PTDN-GO-DBA particle.

A telechelic poly(ethylene glycol) with dopamine and azide functional groups was synthesized and conjugated to the surface of graphene oxide by nitrene [2 + 1] cycloaddition reaction. In order to synthesize the telechelic polymer, cyanuric chloride was conjugated to the end functional group of poly(ethylene glycol) monomethyl ether and the product was reacted with dopamine. Nucleophilic substitution of the chloride group of dopamine-functionalized poly(ethylene glycol) by sodium azide resulted in the final telechelic polymer. After conjugation of telechelic polymer to the surface of graphene sheets, 2,5-thiophenediylbis-boronic acid was attached to their catechol groups and 2D nanomaterials with boronic acid functional groups were obtained (Scheme 1).

Telechelic polymer and functionalized graphene sheets were characterized by different spectroscopy and microscopy methods. Figure 1A(a–f) displays IR spectra of PT, PTD, $PTDN_3$, PTDN-GO, 2,5-thiophenediylbisboronic acid, PTDN-GO-DBA, and PTDN-GO-DBA-Mann. In the IR spectrum of PT absorbance bands at 2895, 1611, and 1580 cm^{-1} were assigned to C–H bonds of poly(ethylene glycol) and C=N bonds of triazine ring. The appearance of absorbance bands at 3045–3656 and 2129 cm^{-1} in the IR spectra of PTD and $PTDN_3$ confirmed the successful synthesis of telechelic polymer with catechol and azide functionalities. After conjugation of $PTDN_3$ to nGO, the absorbance band of the azide group disappeared, which is an indicator for the nitrene [2 + 1] cycloaddition reaction. Absorbance bands at 1518 and 652 cm^{-1} and amplified absorbance band of hydroxyl groups at 3050–3560 cm^{-1} in the IR spectra of PTDN-GO-DBA indicated conjugation of 2,5-thiophenediylbis-boronic acid to PTDN-GO. In the IR spectra of PTDN-GO-DBA and PTDN-GO-DBA-Mann, absorbance bands at 620 and 640 cm^{-1}, which belong to the boronate esters, as well as an absorbance band at 980 cm^{-1}, corresponding to the C–S bond, represent conjugation of boronic acid segments to the functionalized graphene sheets.

The structure of PT and PTD was evaluated by ^{1}H- and ^{13}C NMR spectroscopy. Signals of different protons and carbons are depicted in the NMR spectra of these compounds (Figure 1B). Based on these data, a telechelic polymer was successfully synthesized with the desired functionalities.

Synthesized materials were further characterized by elemental analysis (Table 1). Nitrogen, carbon, and hydrogen contents of $PTDN_3$ were in agreement with the calculated amounts (ESI, Table S1, ESI). The low carbon content of nGO showed that it was highly oxidized. The destructed π-conjugated system of nGO resulted in low fluorescence quenching, which was crucial for biosensing by fluorescence signal. According to elemental analysis, the density of functional groups (conjugated polymer) was high and it was one functional group per 6 carbon atoms of nGO (ESI, p 2). After conjugation of 2,5-thiophenediylbisboronic acid to PTDN-GO, the nitrogen content decreased to 1.27%. This nitrogen content indicated that one boronic acid functional group had been attached to each catechol group of PTDN-GO (ESI, p 2). The sulfur content of PTDN-GO-DBA decreased to 1.1%, which indicated the conjugation of 2,5-thiophenediylbis-boronic acid to PTDN-GO. Conjugation of mannose eventually decreased the nitrogen content of PTDN-GO-DBA to 1.24%.

Figure 2a and 2b represents the tapping mode SFM height images of nGO and PTDN-GO-DBA on a freshly cleaved and atomically flat mica surface. The nGO sample had structures with (longest) lateral dimensions 26 ± 10 nm (sheets up to 100 nm also were observed) and heights mostly of 0.8 ± 0.05 nm (error is standard deviation). We attributed those thin sheets to

DOI: 10.1021/acs.langmuir.9b00915
Langmuir 2019, 35, 10461–10474

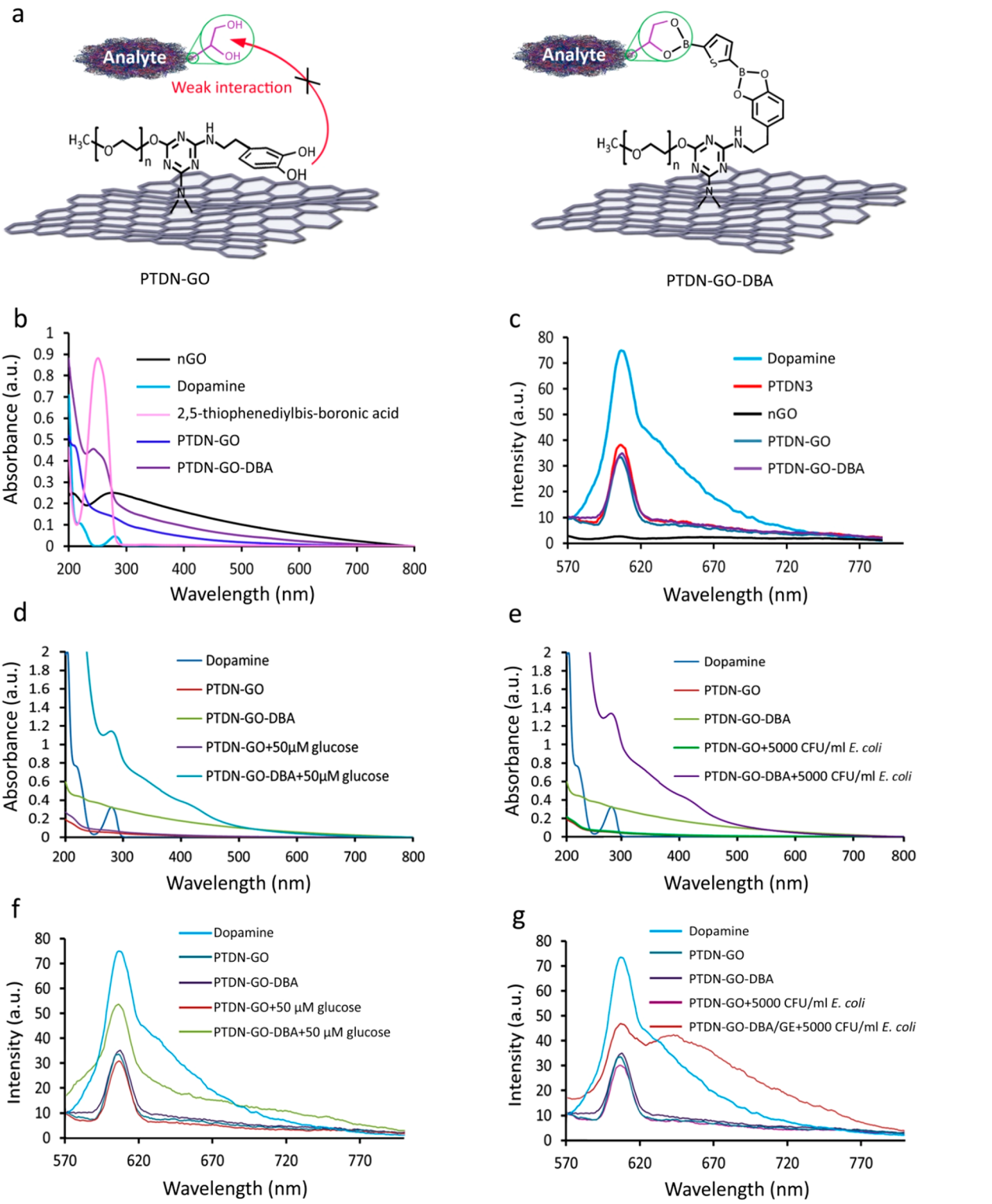

Figure 3. (a) Schematic representation of the interaction between analytes (glucose or *E. coli*) and the functional groups of PTDN-GO (catechol) and PTDN-GO-DBA (boronic acid). (b) UV−vis spectra of nGO, dopamine, 2,5-thiophenediyl bis-boronic acid, PTDN-GO, and PTDN-GO-DBA in water. (c) Fluorescence spectra of dopamine, nGO, $PTDN_3$, PTDN-GO, and PTDN-GO-DBA. Spectra were recorded in PBS (pH 8) with excitation wavelength at 275 nm. UV−vis spectra of PTDN-GO and PTDN-GO-DBA (1 mg/mL) in PBS (pH 8) before and after addition of (d) glucose (50 μM) and (e) *E. coli* (5000 CFU/mL). Fluorescence spectra of PTDN-GO and PTDN-GO-DBA (1 mg/mL) in PBS (pH 8) before and after addition of (f) glucose (50 μM) and (g) *E. coli* (5000 CFU/mL).

single-layer nGO structures. Furthermore, occasionally thicker structures with similar lateral dimensions were also found with heights between 2 and 10 nm. We attributed the thicker structures to possible nGO crystals, which were not yet fully exfoliated in the process of preparation. Similar topographies were found for PTDN-GO-DBA (Figure 2d and 2e). Lateral and height dimensions of PTDN-GO-DBA were increased compared to those for nGO structures. PTDN-GO-DBA exhibited a

DOI: 10.1021/acs.langmuir.9b00915
Langmuir 2019, 35, 10461−10474

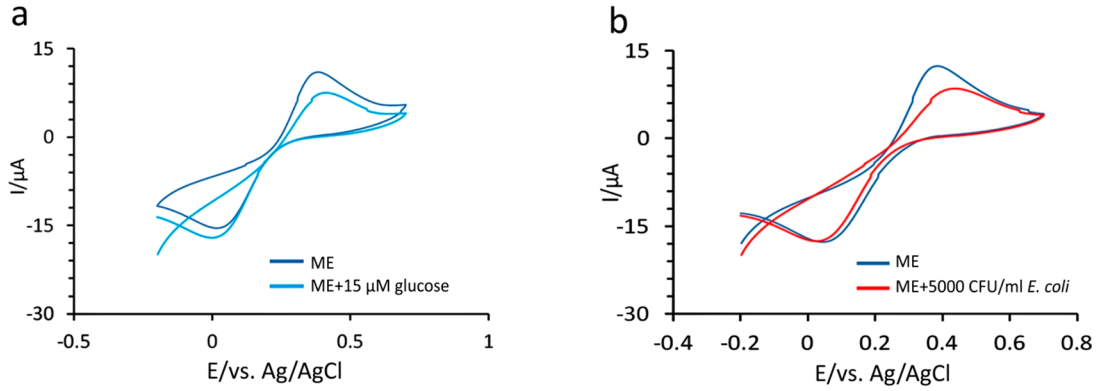

Figure 4. CV of ME (1 mg/mL) after addition of a (a) 15 μM aqueous solution of glucose and (b) 5000 CFU/mL PBS solution of *E. coli*.

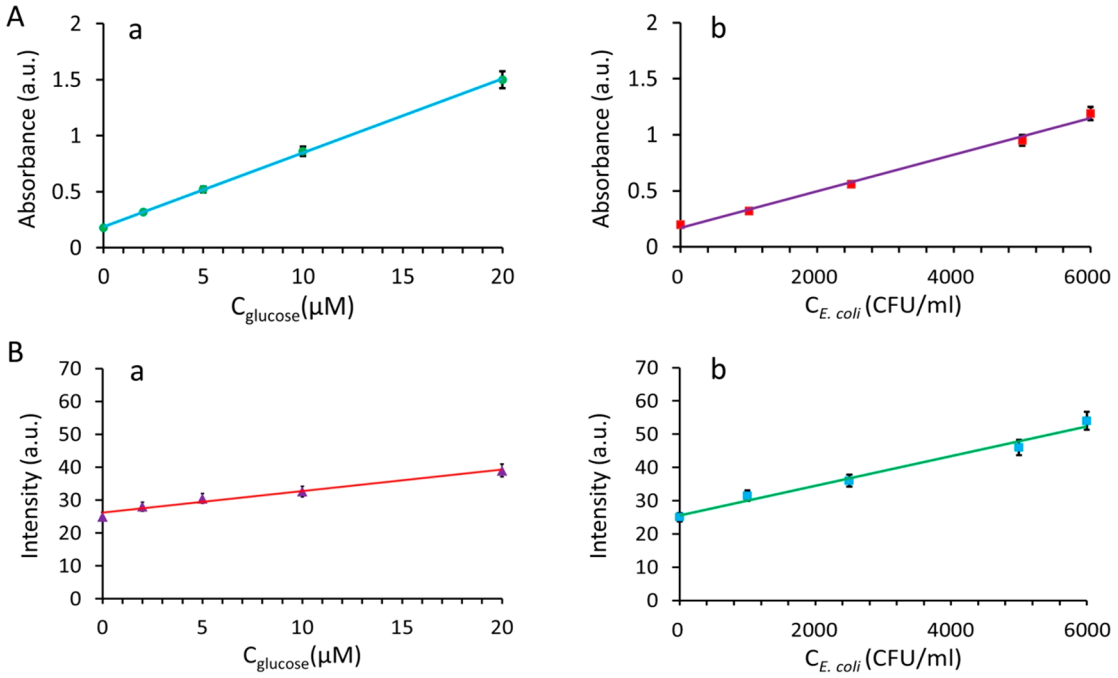

Figure 5. Chart of UV absorption and fluorescence intensity vs glucose and *E. coli* concentrations, increasing the UV absorption and fluorescence emission of PTDN-GO-DBA upon addition of glucose and *E. coli* concentrations. (A) UV−vis absorption and (B) fluorescence intensity after adding (a) an aqueous glucose solution (0, 2, 5, 10, and 20 μM) and (b) a PBS solution of *E. coli* (0, 1000, 2500, 5000, and 6000 CFU/mL). Each experiment was repeated five times (n = 5).

Table 2. Detection Limits for UV, Fluorescence, and Electrochemistry of Glucose, *E. coli*, and Human Blood Serum Containing Glucose and *E. coli* (HBS) (n = 5)[a]

	glucose		*E. coli*		glucose (HBS)		*E. coli* (HBS)	
method	LOD (μM)	RSD	LOD (CFU/mL)	RSD	LOD (μM)	RSD	LOD (CFU/mL)	RSD
UV−vis	2.4	0.04	0.83×10^3	0.04	5.3	0.02	1.20×10^3	0.1
fluorescence	1.9	0.47	0.70×10^3	0.96	2.9	0.23	1.15×10^3	1.78
electrochemistry	2.2	0.08	0.77×10^3	0.07	2.5	0.11	1.07×10^3	0.35

[a] n is the repetitive measurement number.

typical height between 2 and 8 nm. The variation of the heights of different PTDN-GO-DBA sheets was attributed to the polydispersity index (PDI) of PEG chains within these structures and the possibility of attachment of the functionalities to thicker (few layered) nGO crystals. The lateral dimensions of the PTDN-GO-DBA sheets were found to be within 63 ± 10 nm. We attributed the larger lateral sizes of these sheets to the disordered arrangement of the PEG chains within the 2D nGO sheets and lying on the mica surface along the sheet edges (Figure S1, ESI). Therefore, it was possible to assign the increase of the height and lateral dimension of PTDN-GO-DBA sheets to their functionalization.

Since the goal of this work was to construct a biosensor based on the optoelectronic properties of the functionalized graphene oxide sheets, the UV absorption, fluorescence emission, and electrochemical characteristics of the synthesized graphene derivatives were investigated.

DOI: 10.1021/acs.langmuir.9b00915
Langmuir 2019, 35, 10461−10474

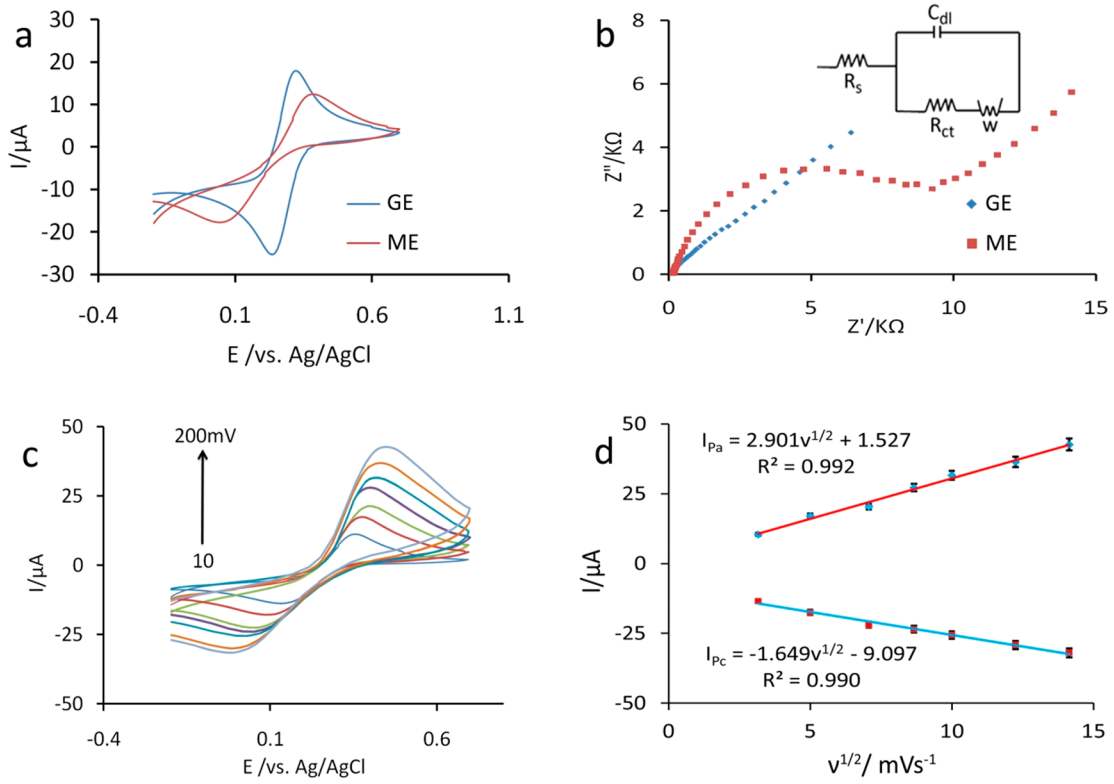

Figure 6. (a) CV and (b) electrochemical impedance spectroscopy (EIS), Nyquist plot, and equivalent circuit (inset) of GE and ME in PBS (pH 8.0) containing $[Fe(CN)_6]^{3-/4-}$ (5 mM) and KCl (0.1M) at a scan rate of 25 mV/s. (c) CV of the ME in PBS (pH 8.0) containing $[Fe(CN)_6]^{3-/4-}$ (5 mM) and KCl (0.1 M) at a scan rate of 10, 25, 50, 75, 100, 150, and 200 mV/s. (d) Linear relationship between the peak current and the square root of the scan rate (10−200 mV/s).

Fluorescence resonance energy transfer (FRET) depends on the electron state[54] of fluorophore and its distance from the platform.[55−58] These properties have been abundantly used for construction of the graphene-based biosensors.[59] Changes in the fluorescence resonance energy transfer, after interactions between analytes and fluorophore, can be used to quantitatively probe various biosystems.[60,61] Yum et al. have shown that interactions between aromatic boronic acids, which are attached to the surface of carbon nanotubes and glucose, change the electronic state of these fluorophores and affect their energy transfer with carbon nanotube.[54] The change in the fluorescence of the carbon nanotube upon this energy transfer has been used to detect glucose.

On the basis of these studies, interactions between biosystems and boronic acid groups are supposed to change the fluorescence of dopamine segments (Figure 3a). PTDN-GO-DBA showed a strong UV absorption at 248 nm, which was assigned to the dopamine and boronic acid segments (Figure 3b). As nGO was highly oxidized, the FRET was not too strong, and a considerable emission for the dopamine segment at 605 nm was observed (Figure 3c). This characteristic is the basis for sensing biosystems by fluorescence signal.

Interactions between targeted biosystems and PTDN-GO-DBA improved the dispersibility and consequently UV absorption of graphene sheets due to the decreased light scattering.[62,63] Accordingly, an increase in the UV absorption of PTDN-GO-DBA at 270 nm, upon addition of glucose and *E. coli*, was used as another signal for detection these biosystems (Figure 3d and 3e, respectively).

To test the reliability of fluorescence and UV signals, an aqueous solution of glucose (50 μM) and a solution of *E. coli* (5000 CFU/mL) in PBS were added to a constant concentration of PTDN-GO and PTDN-GO-DBA in PBS, and their fluorescence and UV spectra were recorded. While addition of glucose and *E. coli* (Figure 3f and 3g, respectively) did not significantly change the fluorescence spectra of PTDN-GO, it did increase the fluorescence intensity of PTDN-GO-DBA at 605 nm dramatically (Figure 3f and 3g).

In addition to fluorescence and UV signals, an electrochemical property of PTDN-GO-DBA was used to detect glucose and *E. coli*. Sulfur atoms of PTDN-GO-DBA are able to improve interactions between the graphene sheets and the gold surfaces. Accordingly, bare gold electrodes (GE) were modified by PTDN-GO-DBA (ME) (Figure S2, ESI), which were then incubated with an aqueous solution of targeted biosystems. The intensity of the current peak in the cyclic voltammograms (CV) of PTDN-GO-DBA was decreased after adding a PBS solution (pH 8.0) of glucose (15 μM) or *E. coli* (5000 CFU/mL) containing 5 mM $[Fe(CN)_6]^{3-/4-}$. The reason for such an observation is the attachment of glucose or *E. coli* to the surface of modified electrode through boronic acid functionalities. This process hinders the diffusion of the $[Fe(CN)_6]^{3-/4-}$ toward the electrode surface, diminishes the electron transfer between analyte and electrode, and causes a decrease in the intensity of the current peak. Such an electrochemical signal is used as an indicator to detect glucose and *E. coli* (Figure 4a and 4b).

Figure 5A and 5B shows raising the intensity of UV absorption and fluorescence emission of PTDN-GO-DBA upon adding different concentrations of glucose and *E. coli*. By extrapolation of these plots to zero, different concentrations of glucose and *E. coli* can be detected. The lowest concentrations of glucose and *E.*

DOI: 10.1021/acs.langmuir.9b00915
Langmuir 2019, 35, 10461−10474

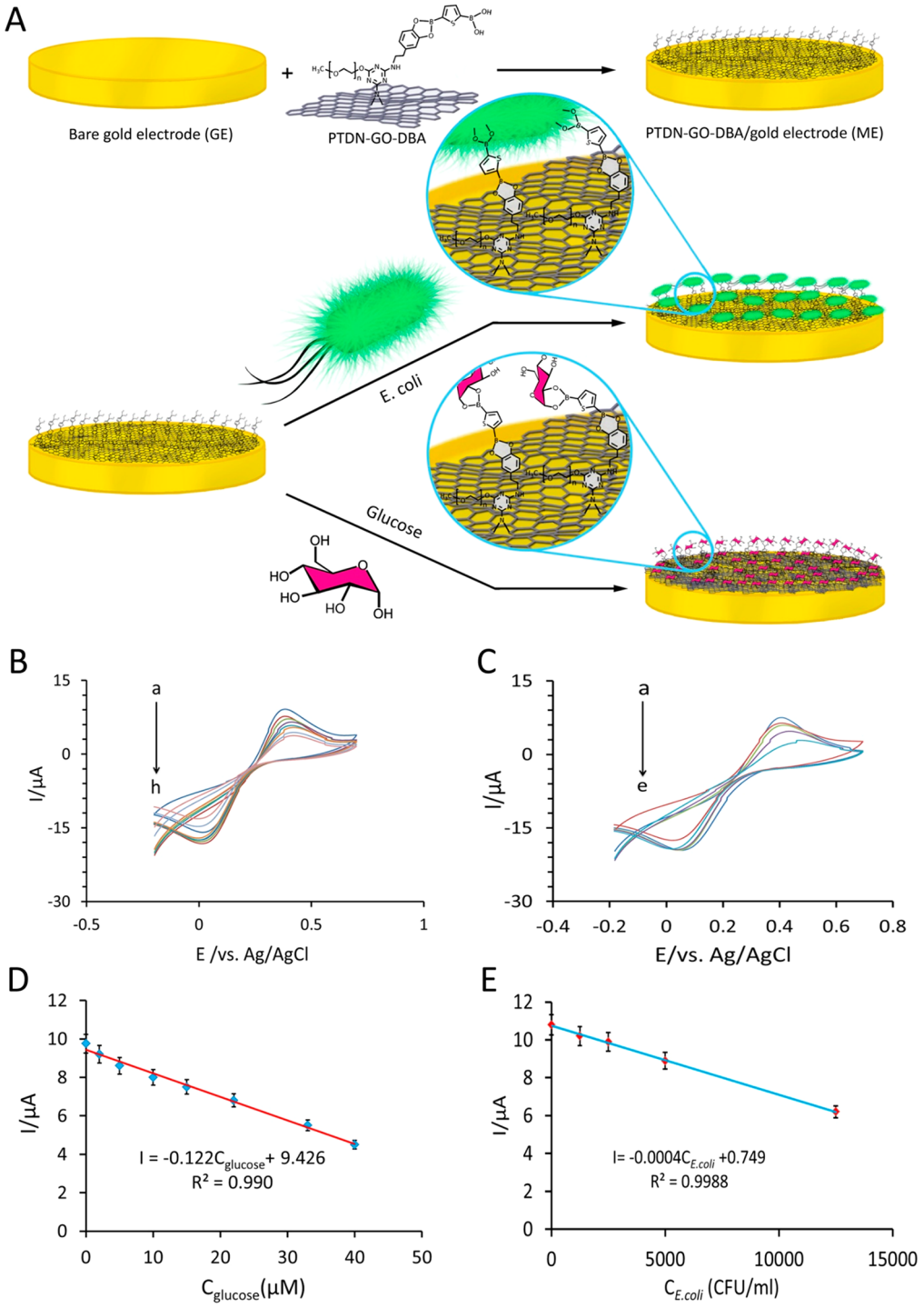

Figure 7. (A) Schematic representation of ME and interaction of glucose and *E. coli* with the boronic acid functional groups of the modified electrode. (B) CV of ME after addition of (a) 0, (b) 2, (c) 5, (d) 10, (e) 15, (f) 22, (g) 33, and (h) 40 μM aqueous solution of glucose containing $[Fe(CN)_6]^{3-/4-}$ solution in PBS (pH 8.0) (5 mM) and KCl (0.1M) at a scan rate of 25 mV/s. (C) CV of ME after addition of (a) 0, (b) 1.25×10^3, (c) 2.5×10^3, (d) 5×10^3, and (e) 1.25×10^4 CFU/mL solution of *E. coli* containing $[Fe(CN)_6]^{3-/4-}$ solution in PBS (pH 8.0) (5 mM) and KCl (0.1M) at a scan rate of 25 mV/s. Linear relationship between the peak current and the concentration of aqueous solutions of (D) glucose (from 0 to 40 μM) and (E) *E. coli* (from 0 to 1.25×10^4 CFU/mL).

coli (detection limit) that was detected by UV and fluorescence signals are shown in Table 2.

In order to investigate the electrochemical sensing in detail, the electrochemical behavior was evaluated for GE before and after modification with PTDN-GO-DBA in PBS (pH8) containing $[Fe(CN)_6]^{3-/4-}$(5 mM) and KCl (0.1 M). Figure 6a demonstrates two well-defined redox peaks with 85 mV potential separations for GE. The CV of ME showed a shift of the oxidation/reduction peak to more negative/positive potentials in comparison to GE, respectively. Also, the observed current response and the shape of the peak of ME were lower than and different from GE, respectively (Figure 6a). Changes in the current and potential peaks were due to the slower electron transfer through the ME.

DOI: 10.1021/acs.langmuir.9b00915
Langmuir 2019, 35, 10461−10474

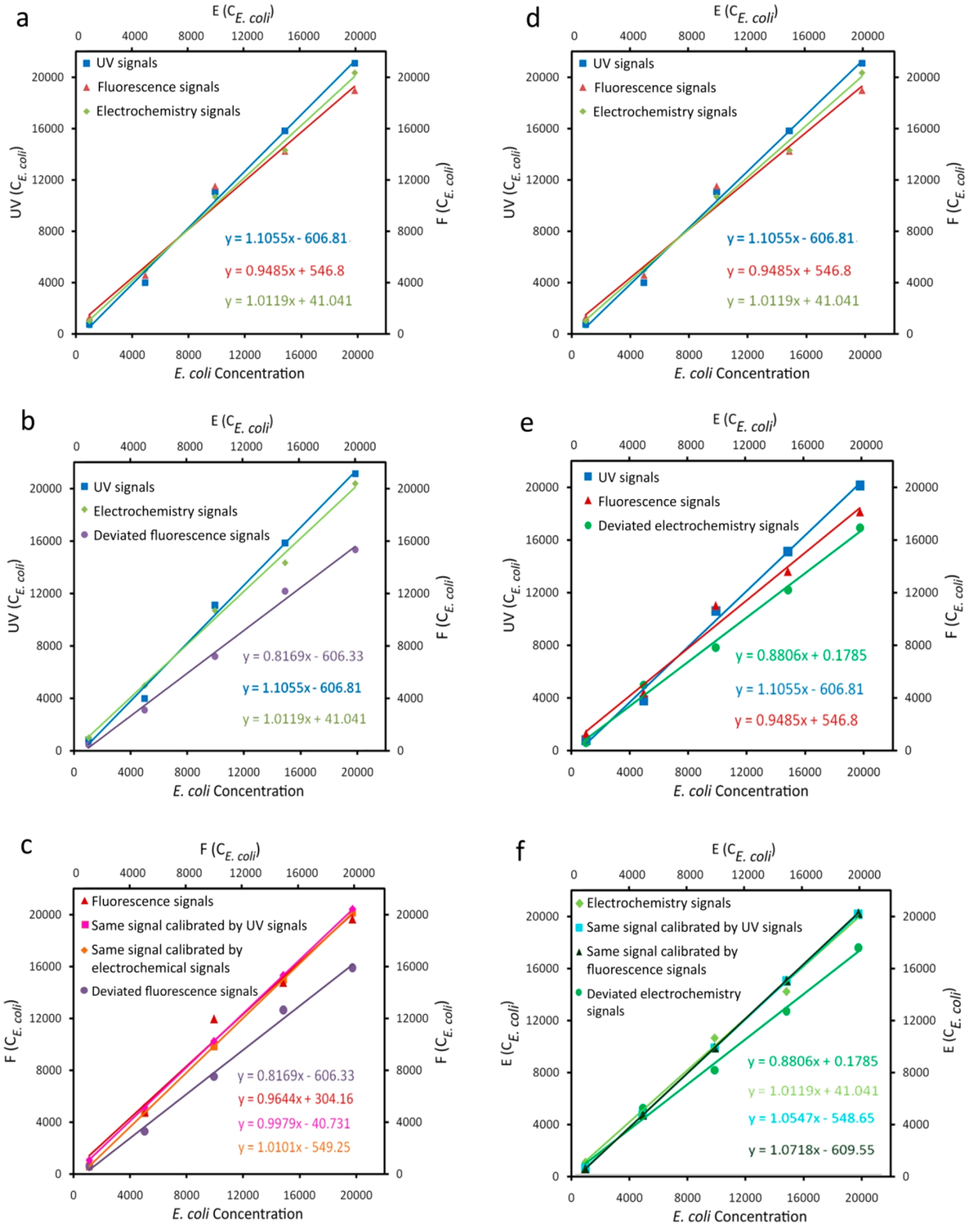

Figure 8. Self-calibration of the fluorescence and electrochemical signals by other signals for detection of *E. coli* (1000−2 × 10^4CFU/mL). (a) UV, fluorescence, and electrochemistry response for detection of different concentrations of *E. coli*. (b) UV, electrochemical, and deviated fluorescence signals for detection of different concentrations of *E. coli*. (c) Fluorescence signal deviated by addition of rhodamine B. Then this signal (the same signal) was corrected by UV and electrochemical signals. (d) UV, fluorescence, and electrochemical signals for detection of different concentration of *E. coli*. (e) UV, fluorescence, and deviated electrochemical signals for detection of different concentration of *E. coli*. (f) Old electrode showed a deviation from the response of the fresh electrode. Deviation of the old electrode was corrected by UV and fluorescence signals.

Electrochemical impedance spectroscopy (EIS) is a useful method for studying the charge transfer and providing good information concerning the conductivity of immobilized layers on the electrode.[64,65]

DOI: 10.1021/acs.langmuir.9b00915
Langmuir 2019, 35, 10461−10474

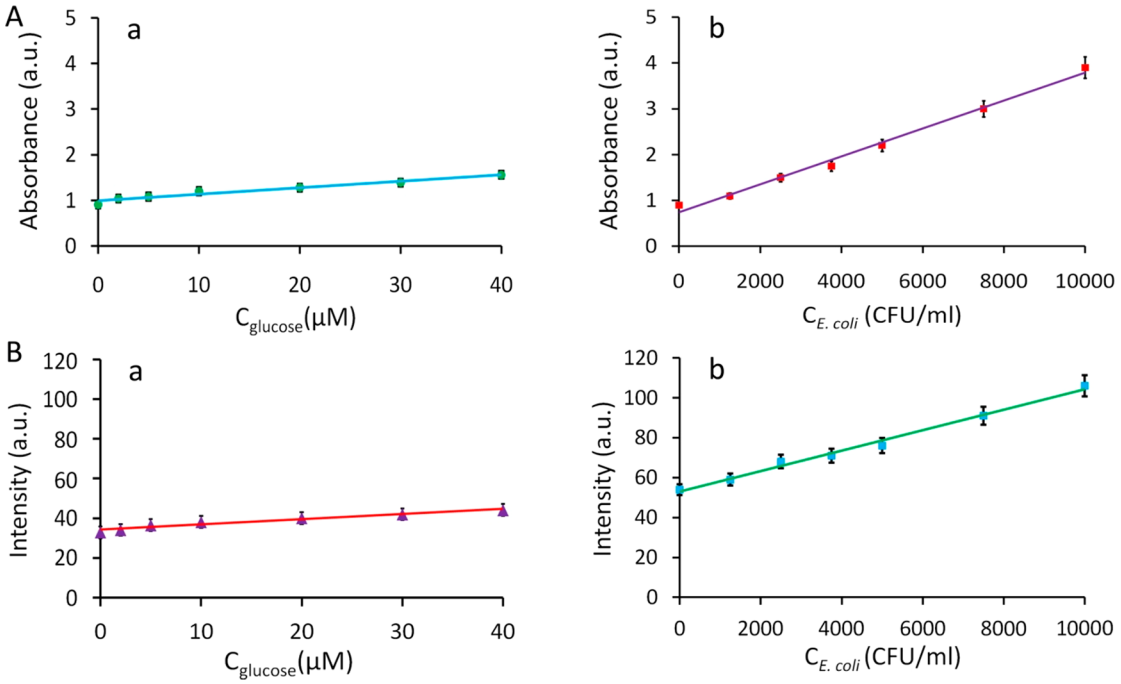

Figure 9. UV absorption and fluorescence intensity vs glucose and *E. coli* concentrations. Intensity of UV absorption and fluorescence emissions of PTDN-GO-DBA upon adding glucose and *E. coli* concentrations increased. (A) UV−vis absorption and (B) fluorescence intensity after adding (a) an aqueous glucose solution (0, 2, 5, 10, 20, 30, and 40 μM) and (b) a PBS solution of *E. coli* (0, 1250, 2500, 3750, 5000, 7500, and 10000 CFU/mL). Each experiment was repeated five times (n = 5).

Accordingly, electrodes were investigated by EIS in $[Fe(CN)_6]^{3-/4-}$ (5 mM) solution containing KCl (0.1 M) (Figure 6b). The resistance of charge transfer (R_{ct}) for ME (9.250 kΩ) was significantly higher than GE (0.552 kΩ) due to the immobilized PTDN-GO-DBA. While GE showed an almost straight line, indicating a diffusion-limited electrochemical behavior, the insulating layer of PTDN-GO-DBA on the electrode surface acted as a barrier to the interfacial electron transfer and led to a semicircular EIS spectrum. The CV curves of this compound were investigated at various scan rates (10−200 mV/s). It was found that the peak current increased along with the rising scan rate. The oxidation and reduction potentials also shifted to more negative and positive values with the increased scan rates, respectively (Figure 6c). At lower scan rates, the cathodic peak current increased linearly with increasing square root of scan rates (Figure 6d). This result indicated that the redox reaction was a surface process and that the ME had good stability and reproducibility. In agreement with EIS results, CVs of ME at different scan rates showed a direct correlation between scan rate and both anodic and cathodic current peaks. This result indicated a diffusion-controlled redox process.

After electrochemical characterization of ME it was applied for the sensing of glucose and *E. coli* (Figure 7A). The modified electrode was exposed to glucose solutions with different concentrations, and CV and EIS were recorded. Clearly, the peak current decreased and peak-to-peak separation increased upon increasing the glucose concentration. Because boronic acid functional groups of PTDN-GO-DBA were immobilized on the electrode and bound to glucose, the effective surface area of the electrode consequently decreased. This process limited diffusion of the redox couple toward the electrode surface (Figure 7B). Also, changes in CV and EIS after applying certain concentrations of *E. coli* proved successful detection of this pathogen by ME (Figure 7C). The current peaks exhibited a linear dependence on the glucose (0−40 μM) and *E. coli* (0−1.25×10^4 CFU/mL) concentrations. Different concentrations of glucose and *E. coli* can be detected by modified electrode using calibration curves in Figure 7D and 7E. The detection of limit (LOD) of the modified electrode for sensing glucose and *E. coli* are shown in Table 2.

One of the main advantages of our biosensor is the simultaneous determination of targets by three different signals. This advantage provided a possibility to test each signal by two other signals and achieving a self-calibrating biosensor. After determination of the concentration of glucose and *E. coli* by electrochemical signal, the same sample was tested by UV and fluorescence signals. Results of self-calibration experiments are shown in Figure 8. As it can be seen, there is a high agreement between the results obtained by different signals. Any error could be detected by deviation from such linear relationship between UV, fluorescence, and electrochemical signals.

The self-calibration feature of the constructed biosensor to detect *E. coli* was investigated by intentional deviation of one signal and consequently correction by two other signals. The fluorescence signal of biosensor, for example, was deviated by adding a certain amount of another fluorescence probe such as Rhodamine B. The fluorescence signal of biosensor was quenched partially by a fluorescence probe, and a deviation from the initial response was induced (Figure 8a and 8b). The deviation of the fluorescence signal was then calculated by UV and electrochemical diagrams and then applied to correct the fluorescence signal. The fluorescence signal corrected by both UV and electrochemical signals (Figure 8c) was in a good agreement with the initial fluorescence signal (Figure 8a), indicating the self-calibration ability of this biosensor. The self-calibration concept was also proven for the electrochemical signal of an old electrode. The signal of the old electrode was

DOI: 10.1021/acs.langmuir.9b00915
Langmuir 2019, 35, 10461−10474

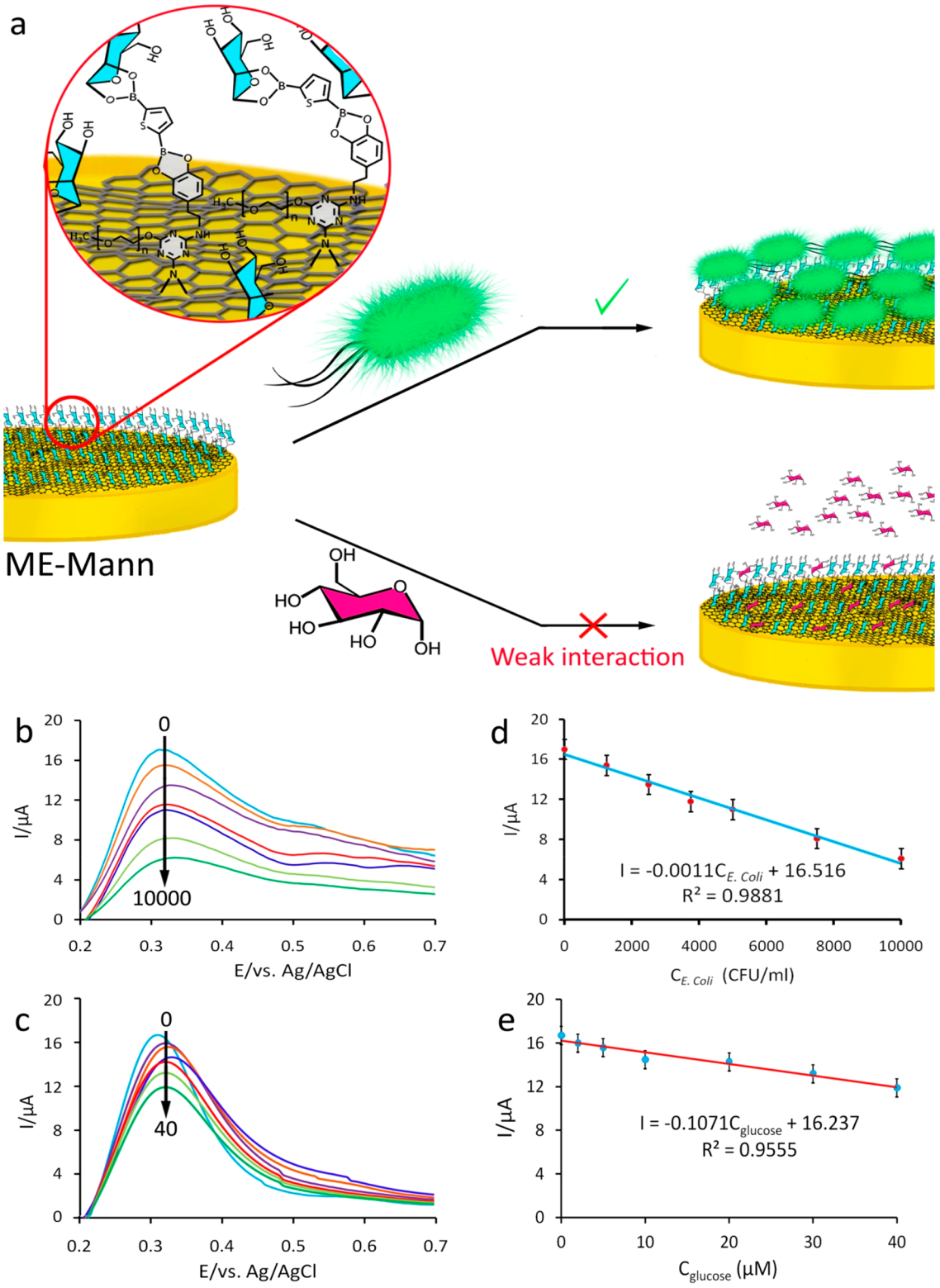

Figure 10. (a) Schematic illustration of ME-Mann and interaction of glucose and *E. coli* with mannose of the modified electrode. DPV curves of ME-Mann containing $[Fe(CN)_6]^{3-/4-}$ (5 mM) and KCl (0.1 M) in PBS (pH 8.0) after addition of human serum containing (b) 0, 1.25×10^3, 2.5×10^3, 3.75×10^3, 5×10^3, 7.5×10^3, and 10^4 CFU/mL *E. coli* and (c) 0, 2, 5, 10, 20, 30, and 40 μM aqueous solution of glucose. Plot of I/μA against E/vs Ag/AgCl, fitted to a linear equation (I and μA represent the current intensity of ME-Mann after addition of human serum containing (d) *E. coli* from 0 to 10^4 CFU/mL) and (e) glucose from 0 to 40 μM.

corrected by UV and fluorescence signals, and the corrected electrochemical signal showed almost the same results as the fresh electrode (Figures 8d–f) (ESI, p 11).

Figure 8 shows that deviation of each signal could be successfully corrected by other signals, leading to a self-calibration property for this biosensor.

DOI: 10.1021/acs.langmuir.9b00915
Langmuir 2019, 35, 10461−10474

Boronic acid-based sensors are generally unselective or show limited selectivity,[66,67] which is also a drawback for our system. To solve this problem mannose was immobilized to PTDN-GO-DBA via *cis*-diol attachment. Since mannose showed specific interactions with *E. coli*,[68−70] the modified biosensor was applied to detect *E. coli* in a complex media.

UV, fluorescence measurements, and differential pulse voltammetry (DPV) were used to investigate the specificity of biosensor to detect *E. coli* in human blood serum (HBS). *E. coli* solutions with known concentrations were mixed with the human blood serum. Then these mixtures were investigated by UV and fluorescence spectroscopy (Figure 9). It was found that the intensity of UV absorption and fluorescence emission of graphene sheets increased upon interactions with *E. coli*. However, these parameters did not considerably change after interaction with glucose. This result proved specific interactions between PTDN-GO-DBA-Mann and *E. coli*. The detection limits of PTDN-GO-DBA-Mann are shown in Table 2.

Differential pulse voltammetry (DPV) was also used for investigating the specificity of the biosensor to detect *E. coli* in human blood serum. *E. coli* samples with known concentrations were mixed with the human blood serum, whereupon the mixture was added to the gold electrode modified by PTDN-GO-DBA-Mann (ME-Mann). Tbe DPV was recorded as well (Figure 10a). DPV of ME-Mann exhibited an oxidation peak at 0.31 V in the absence of *E. coli*. However, a gradual decrease in DPV measurements was observed upon addition of different concentrations of *E. coli* (1.25×10^3−10^4 CFU/mL) (Figure 10b). This is due to the electron-transfer hindering effect caused by *E. coli* immobilized on GE. The linear relationship between the peak current and the *E. coli* concentration with an acceptable correlation coefficient (0.988) showed that this biosensor was able to selectively detect *E. coli* in a complex media with a high accuracy. However, addition of different concentrations of glucose to human blood serums did not significantly decrease the DPV curves of ME-Mann (Figure 10c). This was due to occupation of boronic acids by mannose and therefore weak interaction with glucose. A detection limit as low as 1.3×10^3 CFU/mL was found for sensing *E. coli* in human blood serum by this biosensor.

CONCLUSIONS

The aim of the present study was to prepare a nonenzymatic, self-calibrating, multiresponse, and multifunction biosensor based on functionalized graphene sheets. The biosensor was able to detect biosystems by three different types of signals at the same time. The selectivity of the biosensor toward *E. coli* in a complex medium was improved by attaching mannose to its surface. Taking advantage of the versatility and accuracy of each signal as well as multivalent interactions between the graphene platform and biosystems, functionalized graphene sheets could be used as a powerful, fast-response, and self-examining biosensor.

ASSOCIATED CONTENT

Supporting Information

The Supporting Information is available free of charge on the ACS Publications website at DOI: 10.1021/acs.langmuir.9b00915.

Characterization and supporting data of the materials (PDF)

AUTHOR INFORMATION

Corresponding Author

*E-mail: aadeli@zedat.fu-berlin.de, adeli.m@lu.ac.ir.

ORCID

Jürgen P. Rabe: 0000-0003-0847-6663

Mohsen Adeli: 0000-0001-6895-8491

Author Contributions

Thus project was designed and supervised by M.A. Synthesis of materials and part of the biological studies were performed by S.B. Z.P. performed fluorescence and electrochemistry measurements. M.F.G. and J.P.R. performed SFM studies. A.D.T. helped with characterization of the materials.

Notes

The authors declare no competing financial interest.

ACKNOWLEDGMENTS

The authors thank Dr. Zeinab Pourghobadi for the fluorescence and electrochemistry measurements as well as the Iran Science Elites Federation, the German Science Foundation (DFG), and the Cluster of Excellence "Image Knowledge Gestaltung. An interdisciplinary Laboratory" for financial support. We also to thank the central laboratory (core facility) of Lorestan University for elemental analysis experiments.

ABBREVIATIONS

E. coli, *Escherichia coli*; 2D, two-dimensional; nGO, nanographene oxide; PT, poly(ethylene glycol) monomethyl ether with triazine end group; PTD, dopamine-functionalized PT; $PTDN_3$, azide-functionalized PTD; PTDN-GO, functionalization of nGO by $PTDN_3$; PTDN-GO-DBA, 2,5-thiophenediyl-bisboronic acid-functionalized PTDN-GO; PTDN-GO-DBA-Mann, mannose-functionalized PTDN-GO-DBA; PBS, phosphate buffer saline; FTIR, Fourier transform infrared; UV−vis, ultraviolet−visible; SFM, scanning force microscopy; PDI, polydispersity index; FRET, fluorescence resonance energy transfer; GE, bare gold electrode; ME, modified GE by PTDN-GO-DBA; CV, cyclic voltammograms; EIS, electrochemical impedance spectroscopy; LOD, detection of limit; HBS, human blood serum; DPV, differential pulse voltammetry; ME-Mann, GE modified by PTDN-GO-DBA-Mann

REFERENCES

(1) Rodriguez-Delgado, M. M.; Aleman-Nava, G. S.; Rodriguez-Delgado, J. M.; Dieck-Assad, G.; Martinez-Chapa, S. O.; Barcelo, D.; Parra, R. Laccase-based biosensors for detection of phenolic compounds. *TrAC, Trends Anal. Chem.* **2015**, *74*, 21−45.

(2) Bhalla, N.; Jolly, P.; Formisano, N.; Estrela, P. Introduction to biosensors. *Essays Biochem.* **2016**, *60* (1), 1−8.

(3) Murugaiyan, S. B.; Ramasamy, R.; Gopal, N.; Kuzhandaivelu, V. Biosensors in clinical chemistry: An overview. *Adv. Biomed. Res.* **2014**, *3*, 67.

(4) Xiao, F.; Wang, L.; Duan, H. Nanomaterial based electrochemical sensors for *in vitro* detection of small molecule metabolites. *Biotechnol. Adv.* **2016**, *34* (3), 234−249.

(5) Nagaraj, V. J.; Aithal, S.; Eaton, S.; Bothara, M.; Wiktor, P.; Prasad, S. NanoMonitor: a miniature electronic biosensor for glycan biomarker detection. *Nanomedicine* **2010**, *5* (3), 369−378.

(6) Du, Y.; Dong, S. Nucleic acid biosensors: Recent advances and perspectives. *Anal. Chem.* **2017**, *89* (1), 189−215.

(7) Ray, S.; Panjikar, S.; Anand, R. Structure guided design of protein biosensors for phenolic pollutants. *ACS Sensors* **2017**, *2* (3), 411−418.

(8) Yoo, S. M.; Lee, S. Y. Optical biosensors for the detection of pathogenic microorganisms. *Trends Biotechnol.* **2016**, *34* (1), 7−25.

DOI: 10.1021/acs.langmuir.9b00915
Langmuir 2019, 35, 10461−10474

(9) Seven, B.; Bourourou, M.; Elouarzaki, K.; Constant, J. F.; Gondran, C.; Holzinger, M.; Cosnier, S.; Timur, S. Impedimetric biosensor for cancer cell detection. *Electrochem. Commun.* **2013**, *37*, 36−39.
(10) Gutes, A.; Carraro, C.; Maboudian, R. Single-layer CVD-grown graphene decorated with metal nanoparticlesas a promising biosensing platform. *Biosens. Bioelectron.* **2012**, *33*, 56−59.
(11) Yang, G.; Zhu, C.; Du, D.; Zhu, J.; Lin, Y. Graphene-like two-dimensional layered nanomaterials: applications in biosensors and nanomedicine. *Nanoscale* **2015**, *7*, 14217−14231.
(12) Shavanova, K.; Bakakina, Y.; Burkova, I.; Shtepliuk, I.; Viter, R.; Ubelis, A.; Beni, V.; Starodub, N.; Yakimova, R.; Khranovskyy, V. Application of 2D non-graphene materials and 2D oxide nanostructures for biosensing technology. *Sensors* **2016**, *16*, 223.
(13) Goldsmith, B. R.; Locascio, L.; Gao, Y.; Lerner, M.; Walker, A.; Lerner, J.; Kyaw, J.; Shue, A.; Afsahi, S.; Pan, D.; Nokes, J.; Barron, F. Digital biosensing by foundry-fabricated graphene sensors. *Sci. Rep.* **2019**, *9*, 434.
(14) Song, Y.; Xu, T.; Xu, L. P.; Zhang, X. Nanodendritic gold/graphene-based biosensor for tri-mode miRNA sensing. *Chem. Commun. (Cambridge, U. K.)* **2019**, *55* (12), 1742−1745.
(15) Lebedev, A. A.; Davydov, V. Y.; Novikov, S. N.; Litvin, D. P.; Makarov, Y. N.; Klimovich, V. B.; Samoilovich, M. P. Graphene-based biosensors. *Tech. Phys. Lett.* **2016**, *42* (14), 729−732.
(16) Wang, Y.; Shao, Y.; Matson, D. W.; Li, J.; Lin, Y. Nitrogen-doped graphene and its application in electrochemical biosensing. *ACS Nano* **2010**, *4*, 1790−1798.
(17) Zhu, C.; Du, D.; Lin, Y. Graphene and graphene-like 2D materials for optical biosensing and bioimaging: a review. *2D Mater.* **2015**, *2*, 032004.
(18) Justino, C. I. L.; Gomes, A. R.; Freitas, A. C.; Duarte, A. C.; Rocha-Santos, T. A. P. Graphene based sensors and biosensors. *TrAC, Trends Anal. Chem.* **2017**, *91*, 53−66.
(19) Samuels, A. J.; Carey, J. D. Engineering graphene conductivity for flexible and high-frequency applications. *ACS Appl. Mater. Interfaces* **2015**, *7* (40), 22246−22255.
(20) Ke, Q.; Wang, J. Graphene-based materials for supercapacitor electrodes e A review. *J. Materiomics.* **2016**, *2*, 37−54.
(21) Taguchi, M.; Ptitsyn, A.; Mc Lamore, E. S.; Claussen, J. C. Nanomaterial-mediated biosensors for monitoring glucose. *J. Diabetes Sci. Technol.* **2014**, *8* (2), 403−411.
(22) Viswanathan, S.; Narayanan, T. N.; Aran, K.; Fink, K. D.; Paredes, J.; Ajayan, P.; Filipek, S.; Miszta, P.; Tekin, H. C.; Inci, F.; Demirci, U.; Li; Bolotin, K. I.; Liepmann, D.; Renugopalakrishanan, V. Graphene-protein field effect biosensors: glucose sensing. *Mater. Today* **2015**, *18* (9), 513−522.
(23) Filip, J.; Kasák, P.; Tkac, J. Graphene as a signal amplifier for preparation of ultrasensitive electrochemical biosensors. *Chem. Zvesti.* **2015**, *69* (1), 112−133.
(24) Guday, G.; Donskyi, I. S.; Gholami, M. F.; Algara-Siller, G.; Witte, F.; Lippitz, A.; Unger, W. E. S.; Paulus, B.; Rabe, J. P.; Adeli, M.; Haag, R. Scalable Production of Nanographene and Doping via Nondestructive Covalent Functionalization. *Small* **2019**, *15* (12), No. 1805430.
(25) Georgakilas, V.; Tiwari, J. N.; Kemp, K. C.; Perman, J. A.; Bourlinos, A. B.; Kim, K. S.; Zboril, R. Non-covalent functionalization of graphene and graphene oxide for energy Materials, biosensing, catalytic, and biomedical applications. *Chem. Rev.* **2016**, *116* (9), 5464−5519.
(26) Tu, Z.; Wycisk, V.; Cheng, C.; Chen, W.; Adeli, M.; Haag, R. Functionalized graphene sheets for intracellular controlled release of therapeutic agents. *Nanoscale* **2017**, *9* (47), 18931−18939.
(27) Zhang, J.; Xu, Y.; Cui, L.; Fu, A.; Yang, W.; Barrow, C.; Liu, J. Mechanical properties of graphene films enhanced by homo-telechelic functionalized polymer fillers via π-π stacking interactions. *Composites, Part A* **2015**, *71*, 1−8.
(28) Tan, K. H.; Sattari, S.; Beyranvand, S.; Faghani, A.; Ludwig, K.; Schwibbert, K.; Böttcher, C.; Haag, R.; Adeli, M. Thermoresponsive Amphiphilic Functionalization of Thermally Reduced Graphene Oxide to Study Graphene/Bacteria Hydrophobic Interactions. *Langmuir* **2019**, *35* (13), 4736−4746.
(29) Tan, K. H.; Sattari, S.; Donskyi, I. S.; Cuellar-Camacho, J. L.; Cheng, C.; Schwibbert, K.; Lippitz, A.; Unger, W. E. S.; Gorbushina, A.; Adeli, M.; Haag, R. Functionalized 2D nanomaterials with switchable binding to investigate graphene-bacteria interactions. *Nanoscale* **2018**, *10*, 9525−9537.
(30) Zhou, J.; Huang, Y.; Chen, C.; Xiao, A.; Guo, T.; Guan, B. O. Improved detection sensitivity of γ-aminobutyric acid based on graphene oxide interface on an optical microfiber. *Phys. Chem. Chem. Phys.* **2018**, *20*, 14117−14123.
(31) Mahmoudi, M. Debugging Nano-Bio Interfaces: Systematic Strategies to Accelerate Clinical Translation of Nanotechnologies. *Trends Biotechnol.* **2018**, *36* (8), 755−769.
(32) Mahmoudi, M. Antibody orientation determines corona mistargeting capability. *Nat. Nanotechnol.* **2018**, *13*, 775.
(33) Tu, Z.; Guday, G.; Adeli, M.; Haag, R. Multivalent interactions between 2D nanomaterials and biointerfaces. *Adv. Mater.* **2018**, *30* (13), 1706709.
(34) Gholami, M. F.; Lauster, D.; Ludwig, K.; Storm, J.; Ziem, B.; Severin, N.; Böttcher, C.; Rabe, J. P.; Herrmann, A.; Adeli, M.; Haag, R. Functionalized Graphene as Extracellular Matrix Mimics: Toward Well-Defined 2D Nanomaterials for Multivalent Virus Interactions. *Adv. Funct. Mater.* **2017**, *27*, 1606477.
(35) Faghani, A.; Donskyi, I. S.; Fardin Gholami, M.; Ziem, B.; Lippitz, A.; Unger, W. E. S.; Bottcher, C.; Rabe, J. P.; Haag, R.; Adeli, M. Controlled covalent functionalization of thermally reduced graphene oxide to generate defined bifunctional 2D nanomaterials. *Angew. Chem.* **2017**, *129*, 2719−2723.
(36) Chang, L.; Wu, H.; He, X.; Chen, L.; Zhang, Y. A highly sensitive fluorescent turn-*on* biosensorforglycoproteins basedonboronic acid functional polymer capped Mn-doped ZnS quantum dots. *Anal. Chim. Acta* **2017**, *995*, 91−98.
(37) Li, M.; Zhu, W.; Marken, F.; James, T. D. Electrochemical sensing using boronic acids. *Chem. Commun.* **2015**, *51*, 14562−14573.
(38) Le Brun, A. P.; Clifton, L. A.; Halbert, C. E.; Lin, B.; Meron, M.; Holden, P. J.; Lakey, J. H.; Holt, S. A. Structural characterization of a model gram-negative bacterial surface using lipopolysaccharides from rough strains of *Escherichia coli*. *Biomacromolecules* **2013**, *14*, 2014−2022.
(39) Amin, R.; Elfeky, S. A. Fluorescent sensor for bacterial recognition. *Spectrochim. Acta, Part A* **2013**, *108*, 338−341.
(40) Zhang, Y.; Ma, R.; Zhen, X.; Kudva, Y.; Buhlmann, P.; Koester, S. J. Capacitive sensing of glucose in electrolytes using graphene quantum capacitance varactors. *ACS Appl. Mater. Interfaces* **2017**, *9* (44), 38863−38869.
(41) Zhu, Y.; Hao, Y.; Adogla, E. A.; Yan, J.; Li, D.; Xu, K.; Wang, Q.; Hone, j.; Lin, Q. A. graphene-based affinity nanosensor for detection of low molecular weight molecules. *Nanoscale* **2016**, *8*, 5815−5819.
(42) Scarano, W.; Lu, H.; Stenzel, M. H. Boronic acid ester with dopamine as a tool for bioconjugation and for visualization of cell apoptosis. *Chem. Commun.* **2014**, *50*, 6390−6393.
(43) Rangel-Barajas, C.; Coronel, I.; Florán, B. Dopamine receptors and neurodegeneration. *Aging Dis.* **2015**, *6* (5), 349−368.
(44) Pradhan, T.; Jung, H. S.; Jang, J. H.; Kim, T. W.; Kang, C.; Kim, J. S. Chemical sensing of neurotransmitters. *Chem. Soc. Rev.* **2014**, *43*, 4684−4713.
(45) Chai, L.; Zhou, J.; Feng, H.; Tang, C.; Huang, Y. Y.; Qian, Z. S. Functionalized carbon quantum dots with dopamine for tyrosinase activity monitoring and inhibitor screening: *in Vitro* and intracellular investigation. *ACS Appl. Mater. Interfaces* **2015**, *7* (42), 23564−23574.
(46) Mabuchi, M.; Shimada, J.; Okamoto, K.; Kawakami, Y.; Fujita, S.; Matsushige, K. Time-resolved fluorescence spectroscopy of dopamine in the single cells. *Proc. SPIE* **2001**, *4252*, 140−148.
(47) Wang, H. Y.; Sun, Y.; Tang, B. Study on fluorescence property of dopamine anddetermination of dopamine by fluorimetry. *Talanta* **2002**, *57*, 899−907.

DOI: 10.1021/acs.langmuir.9b00915
Langmuir 2019, 35, 10461−10474

(48) Yildirim, A.; Bayindir, M. Turn-on fluorescent dopamine sensing based on *in situ* formation of visible light emitting polydopamine nanoparticles. *Anal. Chem.* **2014**, *86* (11), 5508−5512.
(49) Chen, S. M.; Peng, K. T. The electrochemical properties of dopamine, epinephrine, norepinephrine, and their electrocatalytic reactions on cobalt (II) hexacyanoferrate films. *J. Electroanal. Chem.* **2003**, *547* (2), 179−189.
(50) Acciaroli, G.; Vettoretti, M.; Facchinetti, A.; Sparacino, G. Calibration of minimally invasive continuous glucose monitoring sensors: state-of-the-art and current perspectives. *Biosensors* **2018**, *8*, 24.
(51) Tu, Z.; Achazi, K.; Schulz, A.; Mülhaupt, R.; Thierbach, S.; Rühl, E.; Adeli, M.; Haag, R. Combination of Surface Charge and Size Controls the Cellular Uptake of Functionalized Graphene Sheets. *Adv. Funct. Mater.* **2017**, *27*, 1701837−1701848.
(52) Tu, Z.; Wycisk, V.; Cheng, C.; Chen, W.; Adeli, M.; Haag, R. Functionalized graphene sheets for intracellular controlled release of therapeutic agents. *Nanoscale* **2017**, *9*, 18931−18939.
(53) Tu, Z.; Qiao, H.; Yan, Y.; Guday, G.; Chen, W.; Adeli, M.; Haag, R. Directed graphene based nanoplatforms for hyperthermia-overcoming multiple drug resistance. *Angew. Chem., Int. Ed.* **2018**, *57*, 11198−11202.
(54) Yum, K.; Ahn, J. H.; McNicholas, T. P.; Barone, P. W.; Mu, B.; Kim, J. H.; Jain, R. M.; Strano, M. S. Boronic Acid Library for Selective, Reversible Near-Infrared Fluorescence Quenching of Surfactant Suspended Single-Walled Carbon Nanotubes in Response to Glucose. *ACS Nano* **2012**, *6* (1), 819−830.
(55) Huang, P. J.; Liu, J. DNA-Length-Dependent Fluorescence Signaling on Graphene Oxide Surface. *Small* **2012**, *8* (7), 977−983.
(56) Xu, S.; Hartvickson, S.; Zhao, J. X. Engineering of SiO2-Au-SiO2 Sandwich Nanoaggregates Using a Building Block: Single, Double, and Triple Cores for Enhancement of Near Infrared Fluorescence. *Langmuir* **2008**, *24*, 7492−7499.
(57) Feng, A. L.; You, M. L.; Tian, L.; Singamaneni, S.; Liu, M.; Duan, Z.; Lu, T. J.; Xu, F.; Lin, M. Distance-Dependent Plasmon-Enhanced Fluorescence of Upconversion Nanoparticles using Polyelectrolyte Multilayers as Tunable Spacers. *Sci. Rep.* **2015**, *5*, 7779.
(58) Yuan, H.; Khatua, S.; Zijlstra, P.; Yorulmaz, M.; Orrit, M. Thousand-Fold Enhancement of Single-Molecule Fluorescence Near a Single Gold Nanorod. *Angew. Chem., Int. Ed.* **2013**, *52*, 1217−1221.
(59) Wu, X.; Xing, Y.; Zeng, K.; Huber, K.; Zhao, J. X. Study of Fluorescence Quenching Ability of Graphene Oxide with a Layer of Rigid and Tunable Silica Spacer. *Langmuir* **2018**, *34* (2), 603−611.
(60) Marras, S. A. E.; Kramer, F. R.; Tyagi, S. Efficiencies of fluorescence resonance energy transfer and contact-mediated quenching in oligonucleotide probes. *Nucleic Acids Res.* **2002**, *30* (21), No. 122e.
(61) Hieb, A. R.; D'Arcy, S.; Kramer, M. A.; White, A. E.; Luger, K. Fluorescence strategies for high-throughput quantification of protein interactions. *Nucleic Acids Res.* **2012**, *40* (5), No. e33.
(62) Chauhan, N.; Maekawa, T.; Kumar, D. N. S. Graphene based biosensors-accelerating medical diagnostics to new-dimensions. *J. Mater. Res.* **2017**, *32*, 2860−2882.
(63) Li, K.; Jin, S.; Han, Y.; Li, J.; Chen, H. Improvement in functional properties of soy protein isolate-based film by cellulose nanocrystal-graphene artificial nacre nanocomposite. *Polymers* **2017**, *9*, 321.
(64) Wang, H. C.; Zhou, H.; Chen, B.; Mendes, P. M.; Fossey, J. S.; James, T. D.; Long, Y. T. A bis-boronic acid modified electrode for the sensitive and selective determination of glucose concentrations. *Analyst* **2013**, *138* (23), 7146−7151.
(65) Sacco, A. Electrochemical impedance spectroscopy: Fundamentals and application in dye-sensitized solar cells. *Renewable Sustainable Energy Rev.* **2017**, *79*, 814−829.
(66) Wu, X.; Chen, X. X.; Jiang, Y. B. Recent advances in boronic acid-based optical chemosensors. *Analyst* **2017**, *142*, 1403−1414.
(67) Wu, X.; Li, Z.; Chen, X. X.; Fossey, J. S.; James, T. D.; Jiang, Y. B. Selective sensing of saccharides using simple boronic acidsand their aggregates. *Chem. Soc. Rev.* **2013**, *42*, 8032−8048.
(68) Guo, X.; Kulkarni, A.; Doepke, A.; Halsall, H. B.; Iyer, S.; Heineman, W. R. Carbohydrate-based label-free detection of *Escherichia coli* ORN 178 using electrochemical impedance spectroscopy. *Anal. Chem.* **2012**, *84*, 241−246.
(69) Ma, F.; Rehman, A.; Liu, H.; Zhang, J.; Zhu, S.; Zeng, X. Glycosylation of quinone-fused polythiophene for reagentless and label-free detection of *E. coli*. *Anal. Chem.* **2015**, *87* (3), 1560−1568.
(70) Yazgan, I.; Noah, N. M.; Toure, O.; Zhang, S.; Sadik, O. A. Biosensor for selective detection of *E. coli* in spinachusing the strong affinity of derivatized mannose with fimbrial lectin. *Biosens. Bioelectron.* **2014**, *61*, 266−273.

DOI: 10.1021/acs.langmuir.9b00915
Langmuir 2019, 35, 10461−10474